

Time-dependent volcano source monitoring using interferometric synthetic aperture radar time series: A combined genetic algorithm and Kalman filter approach

M. Shirzaei¹ and T. R. Walter¹

Received 15 February 2010; revised 11 June 2010; accepted 6 July 2010; published 28 October 2010.

[1] Modern geodetic methods allow continuous monitoring of deformation fields of volcanoes. The acquired data contribute significantly to the study of the dynamics of magmatic sources prior to, during and after eruptions and intrusions. In addition to advancing the monitoring techniques, it is important to develop suitable approaches to deal with deformation time series. Here, we present, test and apply a new approach for time-dependent, nonlinear inversion using a combination of a genetic algorithm (GA) and a Kalman filter (KF). The GA is used in the form presented by Shirzaei and Walter (2009), and the KF implementation now allows for the treatment of monitoring data as a full time series rather than as single time steps. This approach provides a flexible tool for assessing unevenly sampled and heterogeneous time series data and explains the deformation field using time-consistent dislocation sources. Following synthetic tests, we demonstrate the merits of time-consistent source modeling for interferometric synthetic aperture radar (InSAR) data available between 1992 and 2008 from the Campi Flegrei volcano in Italy. We obtained multiple episodes of linear velocity for the reservoir pressure change associated with a parabolic surface deformation on the volcano. These data may be interpreted via differential equations as a linear flux to the shallow reservoir that provides new insight into how both the shallow and deep reservoirs communicate beneath Campi Flegrei. The synthetic test and case study demonstrate the robustness of our approach and the ability to track and monitor the source of systems with complex dynamics. It is applicable to time-dependent optimization problems in volcanic and tectonic environments in other tectonic environments in other areas and allows understanding of the spatiotemporal extent of a physical process in quantitative manner.

Citation: Shirzaei, M., and T. R. Walter (2010), Time-dependent volcano source monitoring using interferometric synthetic aperture radar time series: A combined genetic algorithm and Kalman filter approach, *J. Geophys. Res.*, *115*, B10421, doi:10.1029/2010JB007476.

1. Introduction

[2] In past years, there has been significant technical development in the detection of spatiotemporal surface deformation fields. Dense, continuous Global Positioning System (GPS) networks [Segall and Davis, 1997] and interferometric synthetic aperture radar (InSAR) time series [Berardino *et al.*, 2002; Ferretti *et al.*, 2001] provided valuable information about the temporal evolution of deformation fields. These new developments yield daily and monthly deformation measurements with millimeter precision over regional scales [Dixon *et al.*, 2006; King *et al.*, 1995; Segall and Matthews, 1997; Tizzani *et al.*, 2007].

[3] Inverse modeling is a strategy used to characterize the source of the deformation field. A number of different mod-

eling algorithms for inverting deformation data can currently be found in the literature [e.g., Shirzaei and Walter, 2009]. However, these are commonly applied to either short or selected periods and therefore provide merely a “snapshot” of a particular stage of a system. Modern developments in the field of deformation time series require appropriate progress in the inversion tools to explore the full spatiotemporal capacity of the observations. To address this issue, a Kalman filter (KF) technique is introduced into the field of deformation time series analysis. This technique presents a sophisticated advancement from previous, common approaches.

[4] The KF technique has a recursive formulation that is applicable to irregularly sampled data. In its original form, the KF technique is applicable to linear dynamic systems [Grewal and Andrews, 2001; Kalman, 1960]. In the static case, the KF technique corresponds to a sequential least squares adjustment [Hofmann-Wellenhof *et al.*, 2000].

[5] In the geosciences, the linear dynamic KF (LKF) has already been applied to better understand spatiotemporal

¹Section 2.1, Department of Physics of the Earth, German GeoForschungsZentrum, Potsdam, Germany.

variations in fault slip rates, dike intrusion and fault creep history [Fukuda *et al.*, 2004; Ozawa *et al.*, 2004; Segall *et al.*, 2000; Segall and Matthews, 1997].

[6] While this linear approach is valid for some problems, many dynamic systems are inherently nonlinear. Nonlinearity is especially common in the field of geosciences, with processes such as fault slip rates or volcanic deformations. For example, a volcano may inflate prior to an eruption, undergo rapid collapse during an explosion or be affected by periodic flank movement. Therefore, an extension of the KF technique to include slightly nonlinear problems has been applied [e.g., Grewal and Andrews, 2001]. One widely used extension requires linearization of the equations about the estimated parameters for every time step [Grewal and Andrews, 2001; Welch and Bishop, 2001]. The extended KF has been used for time-dependent estimation of stress field, slip rate and aquifer modeling [Leng and Yeh, 2003; McGuire and Segall, 2003; Miyazaki *et al.*, 2006]. This method only performs well, however, if the equations are locally linear. Because of the recursive nature of the KF technique, when this assumption is violated the errors may be distributed and this may lead to biased results.

[7] The KF technique has been combined with other techniques to overcome this limitation. One recent application combines the KF technique with unscented transforms (UT) to propagate the mean and covariance information through a nonlinear function [Julier and Uhlmann, 1997, 2004; Wan and Van Der Merwe, 2000]. The result is free from derivatives and relies on the fact that approximating a probability distribution is more feasible than approximating an arbitrary nonlinear function [Julier and Uhlmann, 2004].

[8] Recently, Fournier *et al.* [2009] implemented this idea using dynamic models of the magmatic source at Okmok volcano. The crucial issue to consider, however, is the initialization task and the selection of so-called hyperparameters, which are generally problem dependent and only manageable by trial and error [Julier and Uhlmann, 2004; T. Fournier, personal communication, 2009]. The power and importance of the KF for time series assessment is well understood, but a sophisticated implementation that is free from assumptions and limitations has unfortunately not yet been elaborated.

[9] As an alternative to overcome these limitations, combination of the KF technique with other tools, such as Monte Carlo, artificial neural network and wavelet transforms [Chou and Wang, 2004; Fukuda *et al.*, 2004; Kato *et al.*, 2009], is a promising approach.

[10] Along these lines, this study presents a novel, time-dependent, nonlinear inversion tool by combining the KF and the GA techniques. The KF technique utilizes the simple form of Kalman [Grewal and Andrews, 2001] and the GA is implemented in an iterated manner combined with a statistical competency test [Shirzaei and Walter, 2009]. By using a sophisticated confidence estimation scheme, we are able to combine the strength of a confident inversion tool with the robustness of a LKF. The implementation of a standard LKF makes this approach relatively easy to apply and makes optimization of the algorithm parameters very straightforward.

[11] We begin by briefly summarizing the GA and LKF approaches. Later, these two methods are combined and the

capacities of a statistic inversion tool and a time varying filter are combined to estimate the dynamics of the system.

[12] Using a synthetic test, we demonstrate the robustness of our approach by apply it to a long deformation time series obtained by small baseline subset (SBAS)-InSAR between 1992 and 2008 at the Campi Flegrei volcano in Italy. A new understanding of the physical process occurring at this volcano is obtained and the source of deformation is monitored through time.

2. Methods

[13] The concepts of both the applied inversion and the filtering approaches are described, followed by a description of the combination of these two approaches.

2.1. Randomly Iterated Search and Statistical Competency Genetic Algorithm

[14] The genetic algorithm (GA) was recently identified as a powerful inversion tool that has the potential to process large data sets in full resolution [Shirzaei and Walter, 2009]. The GA was introduced by Holland [1975] and has been further improved by many subsequent researchers who provided comprehensive summaries of the theory and applications [e.g., Davis, 1987; Goldberg, 1989; Haupt and Haupt, 2004; Rawlins, 1991; Whitley, 1994]. Despite remarkable successes in solving extremely complex optimization problems, the original form of the GA does not provide any information about the quality of the result. Therefore, several researchers made efforts to determine the quality of the solution obtained by the GA [e.g., Carbone *et al.*, 2008; Deb *et al.*, 2000; Zhou *et al.*, 1995]. Recently, Shirzaei and Walter [2009] introduced a sophisticated extension to the GA. This extension is named Randomly Iterated Search and Statistical Competency (RISC) and allows the quality of the optimized parameters to be estimated. In the RISC approach, the optimization algorithm is initialized with reasonable values based on available information. With random repetitions, the degree of freedom and the chance for exploring the vicinity of the optimal solution increases. This statistical approach allows probability distributions and therefore, the confidence region for selected optimization parameters to be explored. RISC-GA was originally applied in binary format [Shirzaei and Walter, 2009]. To speed up the algorithm, however, we implement it here using continuous variables (for the GA with continuous variables [e.g., Haupt and Haupt, 2004]).

[15] For the GA with continuous variables, if b_{lo} and b_{hi} are the lower and upper bands of the unknowns, respectively, the initial population Pop is generated by

$$\text{Pop} = (b_{hi} - b_{lo})p_{rn} + b_{lo} \quad (1)$$

where p_{rn} is a random number uniformly chosen in the range [0, 1]. Compared to the binary version of the GA, other operators (such as pairing, mating and mutation) will guide the algorithm toward the optimum solution (for details, see Haupt and Haupt [2004] and Michalewicz [1994]). The details for implementing the RISC approach with a continuous variable GA are the same as those explained for the binary version; the reader is referred to Shirzaei and Walter [2009] for a more detailed explanation.

2.2. Linear Dynamic Kalman Filter

[16] The LKF addresses the problem of estimating the parameters of a linear, stochastic system with measurements that are a linear functions of the parameters. According to the original form of the LKF, the system dynamic and measurement models, respectively, are formulated as follows [Grewal and Andrews, 2001]:

$$\begin{aligned} X_k &= \Phi_{k-1}X_{k-1} + w_{k-1} \quad , \quad w_k \sim N(0, Q_k) \\ Z_k &= H_kX_k + \nu_k \quad , \quad \nu_k \sim N(0, R_k) \end{aligned} \quad (2)$$

where X and w are $n \times 1$ vectors of the unknowns and associated Gaussian-distributed noise, respectively; Z and ν are $l \times 1$ vectors of observations and the associated noise with Gaussian distribution, respectively; Φ and H are $n \times n$ and $l \times n$ matrices, respectively [Grewal and Andrews, 2001; Kalman, 1960]. A recursive solution for the system of equations (2) can be generated as follows [see Grewal and Andrews, 2001, Table 4.3]:

$$\begin{aligned} \widehat{X}_k^+ &= \widehat{X}_k^- + \overline{K}_k [Z_k - H_k \widehat{X}_k^-] \\ P_k^+ &= [I - \overline{K}_k H_k] P_k^- \\ X_k^- &= \Phi_{k-1} \widehat{X}_{k-1}^+ \\ P_k^- &= \Phi_{k-1} P_{k-1}^- \Phi_{k-1}^T + Q_{k-1} \\ \overline{K}_k &= P_k^- H_k^T [H_k P_k^- H_k^T + R_k]^{-1} \end{aligned} \quad (3)$$

In equation (3), \widehat{X}_k^+ is the posterior estimate, P_k^+ is the posterior covariance, X_k^- is the priori estimate, P_k^- is the priori variance and \overline{K}_k is the Kalman gain matrix.

2.3. Combining RISC-GA and LKF for Time-Dependent Nonlinear Inversion

[17] The evaluation of a combined inversion tool that uses a KF and the GA to explore deformation time series and to estimate the associated deformation source parameters is detailed below.

[18] The approach of a combined RISC-GA and LKF method is best explained by an example. Assume that a spatiotemporal observation $L_k(x, y)$ is sampled at times $k = 1, \dots, T$ and is simulated by a forward model $F(X_k^1, \dots, X_k^n)$ using

$$L_k(x, y) + r_k(x, y) = F(X_k^1, \dots, X_k^n) \quad (4)$$

where, in terms of crustal deformation, F is an analytical solution for a rectangular dislocation source [Okada, 1985], an inflating point source [Mogi, 1958], a pressurized spherical source [McTigue, 1987], or any combination of them; (X_k^1, \dots, X_k^n) are n time-dependent dislocation source parameters; L_k is the surface deformation observation obtained by either continuous GPS data or InSAR time series; and r_k is the time-dependent observation error.

[19] The aim of this method is to reproduce and explain a time series of source parameters, (X_k^1, \dots, X_k^n) with $i = 1, \dots, n$, such that the mean of the squared error is minimized.

[20] The rationale for our approach combining RISC-GA and LKF is composed of three main steps:

[21] In step 1, compute the static, nonlinear inversion of the surface observations at each time j ($1 \leq j \leq T$) using RISC-GA. In this step, equation (4) is inverted to obtain the parameters (X_j^1, \dots, X_j^n) , regardless of the observations before and after time j . First-order information about the parameters is required to specify the initial population using equation (1) (further detail about RISC-GA initialization is given by Shirzaei and Walter [2009]). After repeating this step T times (i.e., the number of samples), we obtain the dislocation source parameters responsible for the observed surface deformation. In addition, this statistical approach provides associated confidence intervals at T time steps. This estimation is optimized at each time step in terms of the spatial mean square error but not necessarily in terms of the temporal mean square error. To also address the temporal error, a further step is necessary, which is detailed below and accomplished based on the LKF method.

[22] In step 2, to perform LKF, we introduce a system of equations based on the previous inversion step. Assuming a time series of the i th parameter and an associated half length of the confidence region takes the forms $\{rg X_{1, \dots, rg}^i\}$ and $\{rg \sigma_{1, \dots, rg}^i\}$, respectively, we may establish the dynamic system model as follows:

$$\begin{aligned} \begin{bmatrix} X_k^i \\ \overline{V}_k^i \end{bmatrix} &= \begin{bmatrix} 1 & \Delta t \\ 0 & 1 \end{bmatrix} \begin{bmatrix} X_{k-1}^i \\ \overline{V}_{k-1}^i \end{bmatrix} + \begin{bmatrix} X^i w_{k-1}^i \\ \nu^i w_{k-1}^i \end{bmatrix}, \\ X^i w_k^i &\sim N(0, Q_X^i), \quad \nu^i w_k^i \sim N(0, Q_V^i) \end{aligned} \quad (5)$$

and the measurements model as follows:

$$[rg X_k^i] = [1] [kf X_k^i] + [\nu_k^i] \quad , \quad \nu_k^i \sim N(0, R^i) \quad , \quad R^i = Q_X^i \quad (6)$$

where

$$\begin{aligned} Q_X^i &= \frac{1}{k-1} \sum_{p=1}^k (rg \sigma_p^i - rg \overline{\sigma})^2 \\ Q_V^i &= \frac{1}{k-1} \sum_{p=1}^k (V_p^i - \overline{V}^i)^2 \\ rg \overline{\sigma} &= \frac{1}{k} \sum_{p=1}^k rg \sigma_p^i \\ \overline{V}^i &= \frac{1}{k} \sum_{p=1}^k V_p^i \\ V_k^i &= \frac{rg X_k^i - rg X_{k-1}^i}{t_k - t_{k-1}} \end{aligned} \quad (7)$$

Comparing equation (6) with (2), it can be seen that the observations are a result of the inversion at step 1. Because the system of equations is linear, we are able to use the LKF. Each dislocation source parameter is considered to be a particle with constant velocity subject to random velocity perturbations which assumes that the fluctuation of the inversion result over time is caused by random noise. The new solution for the parameters in equations (5)–(7) can be obtained via equation (3). This new solution is obtained such that it minimizes the mean of the temporal mean square error. We note, however, that it is likely that the new solution may not perfectly replicate the surface deformation observations meaning that the solution is not optimum in terms of the spatial mean square error, which requires another step in the process.

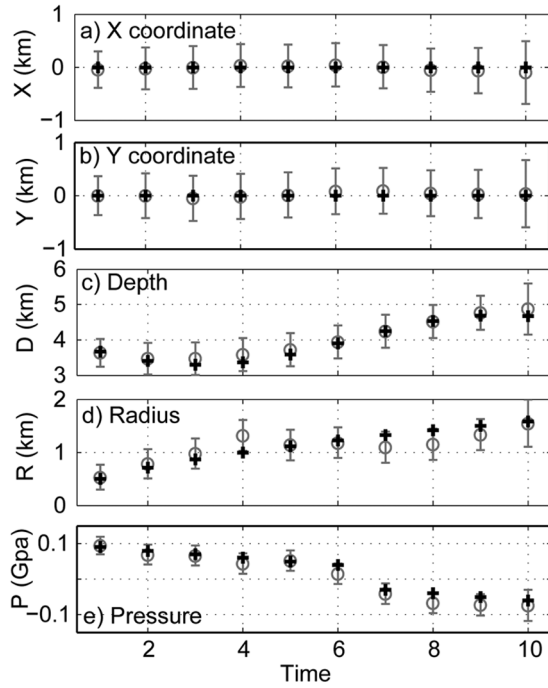


Figure 1. Evaluation of RISC-GA-LKF for a synthetic scenario showing the comparison between the inversion results (open circles with error bars) and the true values (crosses). (a) easting, (b) northing, (c) depth, (d) radius and (e) pressure change of a pressurized, spherical, magmatic source buried in an elastic half-space.

[23] In step 3, to minimize both the spatial and temporal errors, we repeat step 1 with a slight modification: namely that the initial population is divided into two parts. Part one is the priori population (P_{pr}) and is initialized using the same bounds as step 1. Part two is the posterior population (P_{po}), which is initialized using bounds based on the result of step 2. The bounds are described as

$$\begin{aligned}
 {}_{kf}b_{lo}^i &= {}_{kf}\widehat{X}_k^{i+} - P_{11k}^{i+} N_{1-\alpha/2} \\
 {}_{kf}b_{hi}^i &= {}_{kf}\widehat{X}_k^{i+} + P_{11k}^{i+} N_{1-\alpha/2} \\
 P \left[{}_{kf}\widehat{X}_k^{i+} - P_{11k}^{i+} N_{1-\alpha/2} < {}_{rg}X < {}_{kf}\widehat{X}_k^{i+} + P_{11k}^{i+} N_{1-\alpha/2} \right] &< 1 - \alpha
 \end{aligned} \quad (8)$$

where P_{11k}^{i+} is the posterior variance of the estimated parameter ${}_{kf}\widehat{X}_k^{i+}$ and $P[\cdot]$ is the normal probability density function. Equation (8) is defined by the $(1 - \alpha)\%$ confidence interval for the posterior parameters. We use the assumption of a normal probability distribution with bounds defined by the upper and lower limits of the confidence interval. After initialization of the RISC-GA with these two subpopulations, the first based on our priori information and the second based on LKF, we run the RISC-GA again. The GA control parameters (cross over, pairing and mating) may allow random combinations of population members and lead to a result that minimizes both the spatial and temporal mean square errors.

[24] Steps 1–3 are repeated until specified stopping criteria are reached, which may be defined as

$$\begin{aligned}
 \left| \frac{\text{RMSE}^{\text{itr}} - \text{RMSE}^{\text{itr}-1}}{\text{RMSE}^{\text{itr}-1}} \right| &< \varepsilon \\
 \left| \frac{\sum_{i=1}^n \left[\left({}_{kf}\widehat{X}_k^{i+} \right)^{\text{itr}} - \left({}_{kf}\widehat{X}_k^{i+} \right)^{\text{itr}-1} \right]}{\sum_{i=1}^n \left[\left({}_{kf}\widehat{X}_k^{i+} \right)^{\text{itr}-1} \right]} \right| &< \varepsilon
 \end{aligned} \quad (9)$$

where ε is a small arbitrary number, verticals indicate the absolute value operator, and itr denotes the number of iterations. Note that reaching only one of these stopping criteria is sufficient to estimate optimality of the solution.

3. Synthetic Test and Validation

[25] To examine the abilities of the RISC-GA-LKF technique and to ensure that it can improve the stability of the model parameters, we now look at a synthetic test demonstrating its performance. The test requires that five parameters of a dynamic, pressurized, spherical magmatic source be estimated [McTigue, 1987] in an elastic homogeneous half-space. The dynamic models of source depth (D), radius (R) and pressure change (P) are given as

$$\begin{aligned}
 D &= 4 - 0.7 \sin(0.5t) \\
 R &= 0.5\sqrt{t} \quad t = 1 : 1 : 10 \\
 P &= \begin{cases} 0.1 - 0.01t & , \quad t \leq 6 \\ P(6) - 0.01t & , \quad t > 6 \end{cases}
 \end{aligned} \quad (10)$$

As seen in Figure 1, the synthetic models simulate fully nonlinear deformation dynamics, which challenge the ability of the RISC-GA-LKF technique to track such a system. The observation area is a $20 \times 20 \text{ km}^2$ grid with 1 km spacing, and the source location is fixed at coordinate (0,0). To simulate a more realistic scenario, we include random noise with a variance of 1 cm as measurement error. The spatio-temporal deformation field is inverted as follows.

[26] To start the inversion, the RISC-GA is initialized with a population size of 80, mutation rate of 0.7, selection rate of 0.5 and a maximum iteration of 200 [after Shirzaei and Walter, 2009]. The ratio between priori (P_{pr}) and posterior (P_{po}) population size is chosen randomly such that P_{pr} plus P_{po} is equal to the total population size. We use the second relationship shown in equation (7), with $\varepsilon = 0.01$ as a stopping criterion. The upper and lower bounds were chosen to be (−2 km, 2 km) in the horizontal direction, (2 km, 6 km) for the depth, (0 km, 2 km) for the radius and (−0.2 GPa, 0.2 GPa) for the pressure change. These values appear realistic for silicic magmatic systems.

[27] The stopping criteria were reached after three iterations of the algorithm. Figure 1 shows a comparison between the inverted source parameters and the original source parameters. The error bars for the estimated parameters are plotted in the 95% confidence interval. We find that there is good agreement between the original and the estimated parameters. This test shows the merits of the RISC-GA-LKF technique for both tracking systems with nonlinear dynamics, and also for resolving the tradeoff between source parameters such as source radius, pressure

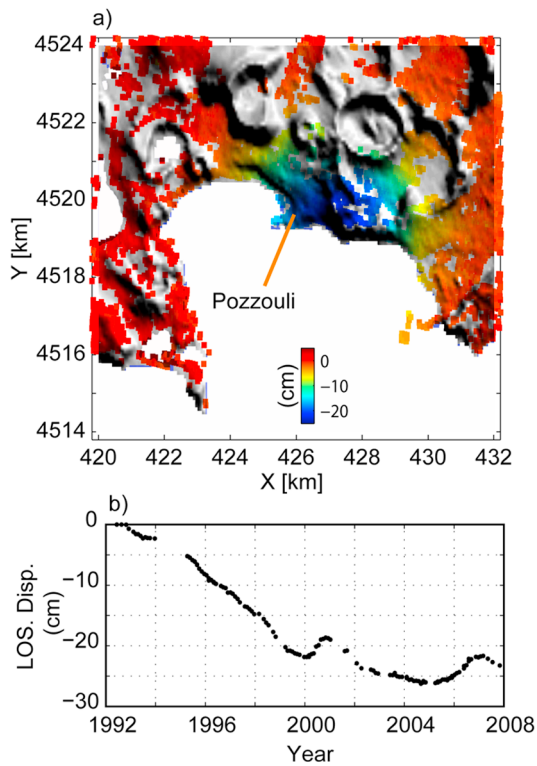


Figure 2. (a) The cumulative displacement of the surface over the study period obtained using the SBAS approach in LOS of a satellite with a descending orbit and a 23° incidence angle and azimuth of 193° [Lanari et al., 2007] and (b) example of the deformation time series at the center of the caldera at Pozzouli.

change and depth. Note that the preselected parameter bounds are merely accelerating the algorithm convergence. If broader bounds are chosen, the algorithm iterations increase at the expense of computation time. However, we found that the final result is mostly independent of the initialization procedure which is a significant advantage of the optimization technique compared to other approaches. (The MATLAB (The MathWorks) script that applies the RISC-GA-KF inversion approach to the synthetic data set is given in auxiliary material Text S1.)¹

4. Application to InSAR Time Series at the Campi Flegrei Volcano

[28] Campi Flegrei (CF) hosts a caldera with a long-documented history of unrest. It is also in one of the most densely populated regions of Italy, partly including the city of Naples and its approximately one million inhabitants. The historical deformation at CF is governed by subsidence at a rate of 1.5 to 1.7 cm/yr, with occasional periods of uplift [Troise et al., 2007]. The most recent large-scale uplift episodes occurred during 1969 to 1972 and 1982 to 1984 [Barberi et al., 1984; Troise et al., 2007].

¹Auxiliary materials are available in the HTML. doi:10.1029/2010JB007476.

[29] The first observation of the deformation at CF using InSAR was reported by Avallone et al. [1999] and associated with a subsidence rate of up to 2.5 cm/yr during the period 1993–1996. Later, using InSAR time series, Lundgren et al. [2001] observed a subsidence rate of 3.5 cm/yr in the period 1993–1998.

[30] Subsequently, further developments of the InSAR time series small base line subset (SBAS) approach allowed the generation of precise spatiotemporal maps of the deformation field to be obtained [Berardino et al., 2002; Lanari et al., 2007]. Later, this deformation time series was extended to late 2008 [Manconi et al., 2010].

[31] Various episodes of the deformation at CF have been studied by many different researchers [see Lanari et al., 2007, and references therein] Although the time series data are available, the dynamics of the source have never been investigated in a temporal context. Thus, InSAR has remained a “snapshot” tool. Utilizing the long time series of the CF deformation field obtained by the SBAS method [Lanari et al., 2007] and our proposed approach for time-dependent source modeling (see above) we study the temporal changes of the reservoir underneath the Campi Flegrei caldera.

[32] To simulate the source of deformation underneath the caldera, we consider a pressurized spherical source in an elastic homogenous half-space (as used in synthetic tests) that evolves over time. The time series used here was provided by Lanari and colleagues at IREA, Naples [Lanari et al., 2007]. The data span the period 1992–2008 and comprises 116 temporal samples with an average sampling rate of 45 days (Figure 2). The deformation field is obtained in the line of sight (LOS) of the satellite with descending orbit and incidence angle of about 23° and an azimuth angle of about 193° . The data were thoroughly validated by comparison to ground truth data, including leveling and GPS data. For data validation, we refer the reader to Lanari et al. [2007]. We considered the observation to be independent in time and space and the observation noise is assumed to be a zero-mean random Gaussian variable with variance of 5 mm. These assumptions reduce the full observation variance-covariance matrix to a diagonal matrix with the observation variance on the main axis.

[33] As seen in Figure 2, the general deformation pattern shows subsidence of up to 25 cm at the center; occasional uplift is apparent mainly in the periods 2001 to 2002 and 2005 to 2007.

[34] For initialization of RISC-GA, we began with 200 iterations, a mutation rate of 0.7, a selection rate of 0.5 and an initial population size of 100. The other parameters in the RISC-GA-LKF were the same as in the synthetic test; the a priori bounds for the parameters are provided in Table 1 and are based on previous studies [see Shirzaei and Walter, 2009, and references therein].

Table 1. Priors Bounds for the Parameters of the Pressurized Spherical Source Used to Simulate the Magmatic Source Underneath Campi Flegrei

| Parameter | X (km) | Y (km) | D (km) | R (km) | P (GPa) |
|-------------|--------|--------|--------|--------|---------|
| Lower bound | 420 | 4515 | 2 | 0.5 | -0.1 |
| Upper bound | 435 | 4525 | 5 | 2 | 0.1 |

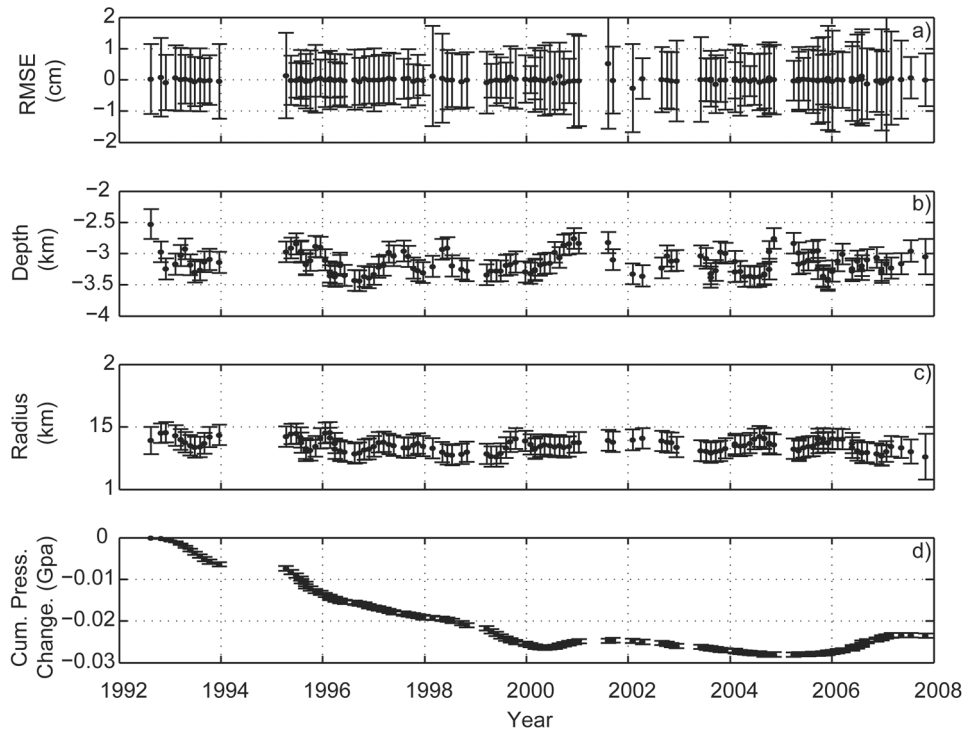


Figure 3. RISC-GA-LKF applied to a deformation time series at the CF volcano. (a) The inversion residual (observation-model) for each snapshot of the deformation time series, (b) time series of the deformation source depth, (c) time series of the deformation source radius, and (d) time series of the deformation source cumulative pressure change. All of the error bars are in the 95% confidence interval.

[35] After four iterations of the RISC-GA-LKF, the stopping criteria were reached and the time series of the magmatic source parameters was obtained. Figure 3 shows the time series of the source parameters (to compare this result with time series obtained by applying only the RISC-GA technique see auxiliary material Figure S1). The easting and northing of the dislocation source position in the UTM map projection system remain relatively stable and are 425 ± 1 km and 425 ± 1.2 km, respectively.

[36] Figure 3a shows the root-mean-square error (RMSE) of the inversion for each time sample with an error bar showing the 95% confidence interval. The RMSE is the normalized total misfit for the entire set of InSAR points at each time step. The magmatic source, with parameters found using the inversion, is able to retrieve the observed deformation time series very well (the spatiotemporal distribution of the inversion residuals are shown at selected time steps in auxiliary material Figure S2).

[37] The cumulative pressure change time series (Figure 3d) emphasizes the overall deflation period of the CF volcano since 1992. Deflation continues until 2000, when the onset of inflation gradually begins and lasts until 2001. After the inflation, another deflation period begins and lasts until late 2005. Beginning in 2006, the gradual deflation period ends and a period of slow inflation begins and lasts, with slight undulations, until the end of the time series.

[38] The magmatic source depth and radius (Figures 3b and 3c) remain nearly stable at 3.1 ± 0.4 km and $1.3 \pm$

0.1 km, respectively. This is the first model obtained for Campi Flegrei with time-consistent parameters.

[39] The limitations and further implications of this approach and results are discussed in section 5.

5. Discussion

[40] We developed and tested a time-dependent, nonlinear inverse modeling method using a combination of the randomly iterated search and statistical competency genetic algorithm (RISC-GA) and a linear Kalman filter (LKF). This novel approach utilizes the advantages of GA for nonlinear inversion and that of the LKF for dynamically estimating source parameter changes in a volcanic system. After showing the merits of the RISC-GA-LKF technique using a synthetic test, we applied it to a deformation time series for the Campi Flegrei caldera between 1992 and 2008, which was obtained using InSAR. Different aspects of this research might be approached as follows.

5.1. Time-Dependent Modeling as the Key for Volcano Source Monitoring

[41] Modern geodetic techniques, such as the GPS and InSAR time series, provide a valuable tool for dynamic monitoring of volcanoes. These data, together with model simulations, allow a better understanding of the volcanic process. Most modeling approaches use snapshots of the deformation rather than exploring the full time series of the deformation field.

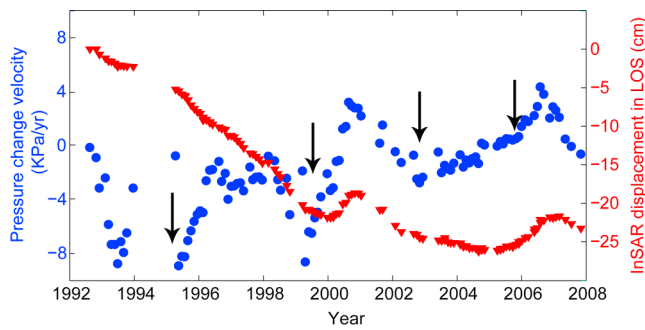


Figure 4. The deformation source pressure change velocity compared to the deformation time series. The major episodes of accelerated change are characterized by a linear trend with a similar slope; the timing of the magma flux is more easily distinguishable based on pressure change velocity than deformation time series.

[42] To address this question, our new approach combines the RISC-GA and the LKF. The rationale for this combination includes the fact that the requirements of a LKF are good a priori estimation of the initial covariance matrix of the parameters and their initial values. We note that these inputs can be provided by any sophisticated optimization tool that is able to provide a reasonable confidence interval for the parameters. Though we prefer the RISC-GA approach implemented here, one should be aware that other optimization techniques might also be applicable. For instance, instead of a GA, other Monte Carlo approaches such as simulated annealing might be used if a precise assessment of the confidence region for the optimum parameters is obtained. In addition, one should ensure that the initial optimization procedure (step 1) is not trapped in local minima, which is the case for gradient base approaches.

[43] The advantages of our approach are as follows: (1) applicability to nonlinear systems; (2) ability to handle irregularly sampled observations; (3) capacity to incorporate heterogeneous observations; (4) recursive manner that allows efficient assessment of new data sets and expanding time series; and (5) less sensitivity to initial values and requirement of only a rough estimation of the search space.

[44] Moreover, the RISC-GA-LKF technique allows the consideration of model deficiency and observation error, which may lead to a more realistic estimate of the confidence interval. This is an advantage when the RISC-GA-LKF technique is compared to other approaches that usually overestimate the quality of the estimated parameters.

[45] The KF implemented here is based upon the assumption that the noise of measurement system behaves randomly. In the presence of colored noise, however, one may replace equation (3) with those explained by *Zimmerman* [1969] for the optimum gain, covariance and parameters that assess the effect of colored noise in a KF.

5.2. Applications for Monitoring the Source Under the Campi Flegrei Volcano

[46] Using the RISC-GA-LKF technique, we modeled the deformation source responsible for 16 years (1992–2008) of unrest underneath CF as a dynamic pressurized spherical

source. The average depth and radius of the source are about 3 km and 1.3 km, respectively, in agreement with previous studies [see *Shirzaei and Walter, 2009*, and references therein].

[47] To estimate the impact of the trade-off between the parameters, we estimated the cross-correlation coefficient between the source depth, pressure change and radius. Pressure change correlates to depth and radius by 2% and 18%, respectively. Radius correlates to depth by 12%. The correlation values are relatively low values and imply that the negative effect of the tradeoff between the source parameters is negligible.

[48] The overall pattern of the cumulative pressure change verifies an apparent contraction period for the source. Reasons for this contraction might include cooling or draining of a reservoir [*De Natale et al., 2006*]. However, the presence of a single shallow reservoir may be too simplistic and may not explain the occasional inflations in the area, such as those seen in 2001 and mid-2006. Those uplift periods might be explained if hydrothermal activities or recharge of the very shallow reservoir are considered [*Battaglia et al., 2006; Gottsmann et al., 2006; Zollo et al., 2008*]. In our work, we did not consider the presence of two sources, or layered or nonlinear rheologies. Nevertheless, our results provide important new insight into how the reservoir pressure evolution works.

[49] Estimation of the velocity of the pressure change indicates four major periods of accelerated change at the magmatic source (Figure 4). The first major period started from the beginning of the observation period and lasted until mid-1993. The second period of accelerated change occurred between 1995 and mid-1996. Both of these episodes are attributed to expedited subsidence at the surface. The next two periods of accelerated pressure change are associated with uplift episodes and took place between 1999 and 2001 and during 2006. These last two episodes of accelerated pressure changes were immediately followed by seismic swarms. For example, the microseismic survey of the 2006 acceleration period shows a cluster of seismic events that occurred at 1.5 to 2.5 km [*Saccorotti et al., 2007*]. Because the seismicity location is somewhat shallower than the inferred reservoir source, it could be speculated whether they are due to reactivation of existing faults above a pressurized reservoir.

[50] Most interestingly, the major episodes of accelerated change are characterized by constant velocity change (i.e., constant acceleration), which exhibits a linear acceleration of about 4.5 to 7 kPa/yr² during the major periods of activity (Figure 5a).

[51] A similar linear magma flux was reported from in situ volcano observatory data. For instance, the Kupaianaha vent on the east rift zone of Kilauea showed a linear magma flux that was found to be associated with a parabolic change in surface deformation [*Denlinger, 1997*]. To investigate whether the CF episodes of linear velocity are associated with parabolic surface deformation, we fit a parabolic function to the deformation time series in a piecewise manner as shown in Figure 5b. There is very good agreement between the deformation time series and the parabolic functions, which might imply that the periods of linear pressure change at the reservoir resulted in parabolic surface

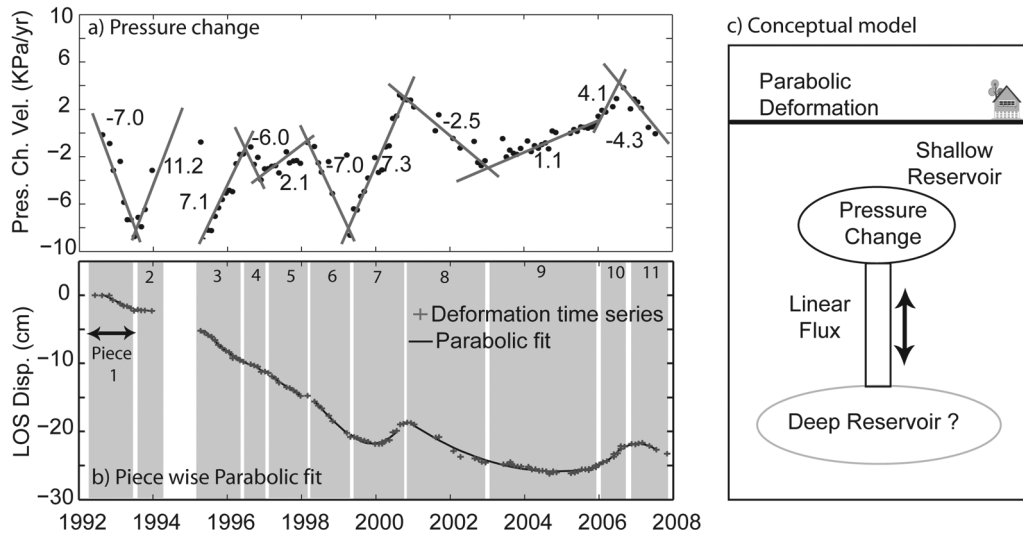


Figure 5. (a) The linear velocity of the pressure change together with the estimated constant acceleration; (b) piecewise parabolic fit to the time series of the surface deformation at CF; and (c) conceptual model explaining the relationship between the deep and shallow reservoirs underneath CF.

deformation. Assuming that V is the reservoir volume and B is the bulk modulus, the following relationship between reservoir pressure change dP and volume change dV holds [Denlinger, 1997]:

$$\frac{dV}{dP} = V/B \quad (11)$$

Assuming an occasional linear flux of bt into the shallow reservoir underneath CF at time t and a constant supply of $a = bt_0$ at time t_0 , the change in the reservoir pressure might be written as follows:

$$\frac{dP}{dt} = -\frac{bB}{V}(t - t_0) \quad (12)$$

Solving this differential equation for P yields

$$P = P_0 - \frac{bB}{2V}(t - t_0)^2 \quad (13)$$

where P_0 is the reservoir pressure at time t_0 . Equation (13) shows that a linear flux into the reservoir through a feeder may cause a parabolic pressure change with linear velocity. Because the surface deformation is a linear function of the pressure change, it also follows a parabolic function. Therefore, the dynamics of long- and short-term uplift and subsidence periods may be controlled by a volume flux, possibly coming from a deeper reservoir into the shallow hydrothermal source.

[52] Seismic tomography underlined the existence of a shallow reservoir and a deep magma chamber beneath CF [Zollo *et al.*, 2008]. However, the way that these two reservoirs communicate is not well understood. Our study suggests that the shallow reservoir at CF is occasionally fed through a vent by a linear flux of material and that the vent might be connected to a deeper reservoir. Figure 5c presents a conceptual model visualizing this hypothesis. This model

implies that the pulses of fluid, or magma flux, from the deeper source to the shallow reservoir are associated with the linear velocity of the pressure change and the parabolic surface deformation at the summit. The trigger might be an external source such as tectonic loading or an internal component such as a pressure change at the deep magma chamber. The effects we observe are the consequence of these triggering mechanisms which demonstrates that monitoring of surface processes may successfully lead to characterizing of the source parameters as a function of time only if changes in the source parameters are physically well understood. New efforts for hazard assessment and early warning may emerge from these findings.

6. Conclusion

[53] We developed and tested a new approach for time-dependent inverse modeling. This approach is a combination of genetic algorithm and Kalman filter. Therefore, it combines the advantages of both technique in terms of efficiency and robustness. This integration allows the consideration of very heterogeneous observations, as well as complex and nonlinear dislocation sources with an efficient processing time that may also be applicable for early warning purposes.

[54] Validation tests were successfully performed on a synthetic example. This simulation highlighted the capabilities of this approach for dynamic modeling of volcano-tectonic deformation sources.

[55] Following the validation test, we applied this approach to a deformation time series obtained at the CF caldera between 1992 and 2008 [Lanari *et al.*, 2007]. The most striking result of this study is the discovery of an approximately fixed source radius (about 1.3 km) as a function of time. Upon inversion, the source pressure change is found to be responsible for a variable deformation field, which often shows different episodes of linear infla-

tion and deflation associated with a parabolic deformation at the surface. This linear pressure change and parabolic deformation was interpreted using differential equations as a linear flux into the shallow reservoir from a deeper magma chamber. This analysis provides new insight into how the deep and shallow reservoirs at CF communicate.

[56] Consequently, we argue that the method presented here has advantages for time series modeling and it is well suited for source monitoring and further applications in volcanic and tectonic fast response systems.

[57] **Acknowledgments.** SBAS-InSAR data utilized in the algorithm test and examples were kindly provided by R. Lanari. M.S. is funded through the Geotechnologies Program "Managing Volcano Unrest." T.R.W. acknowledges a grant from the Emmy-Noether fellowship (WA1642-1/4).

References

- Avallone, A., A. Zollo, P. Briole, C. Delacourt, and F. Beauducel (1999), Subsidence of Campi Flegrei (Italy) detected by SAR interferometry, *Geophys. Res. Lett.*, *26*(15), 2303–2306, doi:10.1029/1999GL900497.
- Barberi, F., et al. (Eds.) (1984), The 1982–1984 Bradysismic crisis at Phlegrean Fields (Italy), *Bull. Volcanol.*, *47*, 173–411, doi:10.1007/BF01961546.
- Battaglia, M., C. Troise, F. Obrizzo, F. Pingue, and G. De Natale (2006), Evidence for fluid migration as the source of deformation at Campi Flegrei caldera (Italy), *Geophys. Res. Lett.*, *33*, L01307, doi:10.1029/2005GL024904.
- Berardino, P., G. Fornaro, R. Lanari, and E. Sansosti (2002), A new algorithm for surface deformation monitoring based on small baseline differential SAR interferograms, *IEEE Trans. Geosci. Remote Sens.*, *40*, 2375–2383, doi:10.1109/TGRS.2002.803792.
- Carbone, D., G. Currenti, and C. Del Negro (2008), Multiobjective genetic algorithm inversion of ground deformation and gravity changes spanning the 1981 eruption of Etna volcano, *J. Geophys. Res.*, *113*, B07406, doi:10.1029/2006JB004917.
- Chou, C. M., and R. Y. Wang (2004), Application of wavelet-based multi-model Kalman filters to real-time flood forecasting, *Hydrol. Processes*, *18*, 987–1008, doi:10.1002/hyp.1451.
- Davis, L. (1987), *Genetic Algorithms and Simulated Annealing*, Pitman, London.
- Deb, K., et al. (2000), A fast elitist nondominated sorting genetic algorithm for multi-objective optimization: NSGA-II, in *Proceedings of the 6th International Conference on Parallel Problem Solving from Nature, Lect. Notes Comput. Sci.*, vol. 1917, pp. 849–85, Springer, New York.
- De Natale, G., C. Troise, F. Pingue, G. Mastrolorenzo, L. Pappalardo, M. Battaglia, and E. Boschi (2006), The Campi Flegrei caldera: Unrest mechanisms and hazards, *Geol. Soc. Spec. Publ.*, *269*, 25–45, doi:10.1144/GSL.SP.2006.269.01.03.
- Denlinger, R. P. (1997), A dynamic balance between magma supply and eruption rate at Kilauea volcano, Hawaii, *J. Geophys. Res.*, *102*, 18,091–18,100, doi:10.1029/97JB01071.
- Dixon, T. H., et al. (2006), Space geodesy: Subsidence and flooding in New Orleans, *Nature*, *441*, 587–588, doi:10.1038/441587a.
- Ferretti, A., C. Prati, and F. Rocca (2001), Permanent scatterers in SAR interferometry, *IEEE Trans. Geosci. Remote Sens.*, *39*, 8–20, doi:10.1109/36.898661.
- Fournier, T., J. Freymueller, and P. Cervelli (2009), Tracking magma volume recovery at Okmok volcano using GPS and an unscented Kalman filter, *J. Geophys. Res.*, *114*, B02405, doi:10.1029/2008JB005837.
- Fukuda, J. I., T. Higuchi, S. Miyazaki, and T. Kato (2004), A new approach to time-dependent inversion of geodetic data using a Monte Carlo mixture Kalman filter, *Geophys. J. Int.*, *159*, 17–39, doi:10.1111/j.1365-246X.2004.02383.x.
- Goldberg, D. E. (1989), *Genetic Algorithms in Search Optimization, and Machine Learning*, Addison-Wesley, Reading, Mass.
- Gottsmann, J., et al. (2006), Spatiotemporal variations in vertical gravity gradients at the Campi-Flegrei caldera (Italy): A case for source multiplicity during unrest?, *Geophys. J. Int.*, *167*, 1089–1096, doi:10.1111/j.1365-246X.2006.03157.x.
- Grewal, M. S., and A. P. Andrews (2001), *Kalman Filtering: Theory and Practice Using MATLAB*, 416 pp., Wiley-Interscience, New York.
- Haupt, R. L., and S. E. Haupt (2004), *Practical Genetic Algorithms*, John Wiley, New York.
- Hofmann-Wellenhof, B., et al. (2000), *Global Positioning System: Theory and Practice*, 5th ed., 390 pp., Springer, New York.
- Holland, J. H. (1975), *Adaptation in Natural and Artificial Systems*, Univ. of Mich. Press, Ann Arbor.
- Julier, S. J., and J. K. Uhlmann (1997), A new extension of the Kalman filter to nonlinear systems, paper presented at 11th International Symposium on Aerospace/Defence Sensing, Simulation and Controls, SPIE, Orlando, Fla.
- Julier, S. J., and J. K. Uhlmann (2004), Unscented filtering and nonlinear estimation, *Proc. IEEE*, *92*, 401–422, doi:10.1109/JPROC.2003.823141.
- Kalman, R. E. (1960), A new approach to linear filtering and prediction problems, *J. Basic Eng.*, *82*, 35–45.
- Kato, Y., M. Kawahara, and N. Koizumi (2009), Kalman filter finite element method applied to dynamic ground motion, *Int. J. Numer. Anal. Methods Geomech.*, *33*, 1135–1151, doi:10.1002/nag.758.
- King, N. E., J. L. Svarc, E. B. Fogleman, W. K. Gross, K. W. Clark, G. D. Hamilton, C. H. Stiffler, and J. M. Sutton (1995), Continuous GPS observations across the Hayward fault, California, 1991–1994, *J. Geophys. Res.*, *100*, 20,271–20,283, doi:10.1029/95JB02035.
- Lanari, R., F. Casu, M. Manzo, G. Zeni, P. Berardino, M. Manunta, and A. Pepe (2007), An overview of the small baseline subset algorithm: A DInSAR technique for surface deformation analysis, *Pure Appl. Geophys.*, *164*, 637–661, doi:10.1007/s00024-007-0192-9.
- Leng, C. H., and H. D. Yeh (2003), Aquifer parameter identification using the extended Kalman filter, *Water Resour. Res.*, *39*(3), 1062, doi:10.1029/2001WR000840.
- Lundgren, P., S. Usai, E. Sansosti, R. Lanari, M. Tesaro, G. Fornaro, and P. Berardino (2001), Modeling surface deformation observed with synthetic aperture radar interferometry at Campi Flegrei caldera, *J. Geophys. Res.*, *106*, 19,355–19,366, doi:10.1029/2001JB000194.
- Manconi, A., T. R. Walter, M. Manzo, G. Zeni, P. Tizzani, E. Sansosti, and R. Lanari (2010), On the effects of 3-D mechanical heterogeneities at Campi Flegrei caldera, southern Italy, *J. Geophys. Res.*, *115*, B08405, doi:10.1029/2009JB007099.
- McGuire, J. J., and P. Segall (2003), Imaging of aseismic fault slip transients recorded by dense geodetic networks, *Geophys. J. Int.*, *155*, 778–788, doi:10.1111/j.1365-246X.2003.02022.x.
- McTigue, D. F. (1987), Elastic stress and deformation near a finite spherical magma body: Resolution of the point source paradox, *J. Geophys. Res.*, *92*, 12,931–12,940, doi:10.1029/JB092iB12p12931.
- Michalewicz, Z. (1994), *Genetic Algorithms + Data Structures = Evolution Programs*, 2nd ed., Springer, New York.
- Miyazaki, S., P. Segall, J. J. McGuire, T. Kato, and Y. Hatanaka (2006), Spatial and temporal evolution of stress and slip rate during the 2000 Tokai slow earthquake, *J. Geophys. Res.*, *111*, B03409, doi:10.1029/2004JB003426.
- Mogi, K. (1958), Relations between the eruptions of various volcanos and the deformations of the ground surfaces around them, *Bull. Earthquake Res. Inst. Univ. Tokyo*, *36*, 99–134.
- Okada, Y. (1985), Surface deformation due to shear and tensile faults in a half-space, *Bull. Seismol. Soc. Am.*, *75*, 1135–1154.
- Ozawa, S., S. Miyazaki, T. Nishimura, M. Murakami, M. Kaidzu, T. Imakiire, and X. Ji (2004), Creep, dike intrusion, and magma chamber deflation model for the 2000 Miyake eruption and the Izu islands earthquakes, *J. Geophys. Res.*, *109*, B02410, doi:10.1029/2003JB002601.
- Rawlins, G. J. E. (1991), *Foundations of Genetics Algorithms*, Morgan Kaufmann, Burlington, Mass.
- Saccorotti, G., et al. (2007), Seismicity associated with the 2004–2006 renewed ground uplift at Campi Flegrei Caldera, Italy, *Phys. Earth Planet. Inter.*, *165*, 14–24, doi:10.1016/j.pepi.2007.07.006.
- Segall, P., and J. Davis (1997), GPS applications for geodynamics and earthquake studies, *Annu. Rev. Earth Planet. Sci.*, *25*, 301–336, doi:10.1146/annurev.earth.25.1.301.
- Segall, P., and M. Matthews (1997), Time dependent inversion of geodetic data, *J. Geophys. Res.*, *102*, 22,391–22,409, doi:10.1029/97JB01795.
- Segall, P., R. Bürgmann, and M. Matthews (2000), Time-dependent triggered afterslip following the 1989 Loma Prieta earthquake, *J. Geophys. Res.*, *105*, 5615–5634, doi:10.1029/1999JB900352.
- Shirzaei, M., and T. R. Walter (2009), Randomly Iterated Search and Statistical Competency (RISC) as powerful inversion tools for deformation source modeling: Application to volcano InSAR data, *J. Geophys. Res.*, *114*, B10401, doi:10.1029/2008JB006071.
- Tizzani, P., et al. (2007), Surface deformation of Long Valley caldera and Mono Basin, California, investigated with the SBAS-InSAR approach, *Remote Sens. Environ.*, *108*, 277–289, doi:10.1016/j.rse.2006.11.015.
- Troise, C., G. De Natale, F. Pingue, F. Obrizzo, P. De Martino, U. Tammara, and E. Boschi (2007), Renewed ground uplift at Campi Flegrei caldera (Italy): New insight on magmatic processes and forecast, *Geophys. Res. Lett.*, *34*, L03301, doi:10.1029/2006GL028545.

- Wan, E. A., and R. Van Der Merwe (2000), The unscented Kalman filter for nonlinear estimation, in *The IEEE 2000 Adaptive Systems for Signal Processing, Communications, and Control Symposium: AS-SPCC, October 1-4, 2000, Chateau Lake Louise, Lake Louise, Alberta, Canada*, pp. 153–158, 10.1109/ASSPCC.2000.882463, IEEE, New York.
- Welch, G., and G. Bishop (2001), *An Introduction to the Kalman Filter*, 81 pp., Univ. of N. C. at Chapel Hill, Chapel Hill.
- Whitley, D. L. (1994), A genetic algorithm tutorial, *Stat. Comput.*, 4, 65–85, doi:10.1007/BF00175354.
- Zhou, R., et al. (1995), Application of genetic algorithm to constrain near-source velocity structure for 1989 Sichuan earthquake, *Bull. Seismol. Soc. Am.*, 85, 590–605.
- Zimmerman, W. (1969), On the optimum colored noise Kalman filter, *IEEE Trans. Autom. Control.*, 14, 194–196, doi:10.1109/TAC.1969.1099149.
- Zollo, A., N. Maercklin, M. Vassallo, D. Dello Iacono, J. Virieux, and P. Gasparini (2008), Seismic reflections reveal a massive melt layer feeding Campi Flegrei caldera, *Geophys. Res. Lett.*, 35, L12306, doi:10.1029/2008GL034242.

M. Shirzaei and T. R. Walter, Section 2.1, Department of Physics of the Earth, German GeoForschungsZentrum, Telegrafenberg, D-14473 Potsdam, Germany. (shirzaei@gfz-potsdam.de)